Ionization of atoms by strong infrared fields: Solution of the time-dependent Schrödinger equation in momentum space for a model based on separable potentials

H. M. Tetchou Nganso,[1,2,*] Yu. V. Popov,[3] B. Piraux,[1,†] J. Madroñero,[4] and M. G. Kwato Njock[2]

[1]*Institute of Condensed Matter and Nanosciences, Université Catholique de Louvain, chemin du cyclotron, 2, B-1348 Louvain-la Neuve, Belgium*

[2]*Centre for Atomic Molecular Physics and Quantum Optics (CEPAMOQ), Faculty of Science, University of Douala, P.O. Box 8580, Douala, Cameroon*

[3]*Nuclear Physics Institute, Moscow State University, Moscow 119991, Russia*

[4]*Physik Department, Technische Universität München, James-Franck-Straße, D-85747 Garching, Germany*

(Received 22 September 2010; published 14 January 2011)

We consider the ionization of atomic hydrogen by a strong infrared field. By starting from the corresponding time-dependent Schrödinger equation in momentum space, we develop a model in which the kernel of the nonlocal Coulomb potential is replaced by a finite sum of separable potentials. Each separable potential supports one bound state of atomic hydrogen. Here, we consider only the $1s$, $2s$, and $2p$ states. In this way, the full three-dimensional Schrödinger equation reduces to a system of a few coupled one-dimensional linear Volterra integral equations. The objective of this first contribution is to give a detailed account of the model and to validate it in physical situations where the dynamics are well understood.

DOI: 10.1103/PhysRevA.83.013401 PACS number(s): 32.80.Rm, 34.10.+x, 32.80.Wr

I. INTRODUCTION

The study of the highly nonlinear interaction of one-electron atoms with intense infrared laser pulses has stimulated the development of numerous mathematical methods and numerical algorithms to solve the corresponding time-dependent Schrödinger equation (TDSE). The numerical solution of the TDSE by means of spectral and finite difference grid methods [1–8] has provided fundamental insights into the basic processes that dominate laser-matter physics in this regime, namely above-threshold ionization (ATI) and high-order harmonic generation (HOHG). However, it is very difficult to draw conclusions regarding the actual mechanisms that lead to these two processes because it is always *after* the laser turnoff that the relevant information is extracted from the numerical solution of the TDSE [9]. Nevertheless, by means of a simple model, Keldysh [10] has shown that depending on the field intensity, we can distinguish two regimes where different mechanisms take place: the perturbative regime at relatively low intensity where multiphoton processes are dominant and the tunneling regime in the strong field limit. More precisely, Keldysh has introduced the adiabaticity parameter $\gamma = \frac{\omega}{E}\sqrt{2I_p}$ where ω is the laser field frequency, E, the field amplitude, and I_p, the ionization potential of the atom. For $\gamma \gg 1$, ATI and harmonic generation occur via multiphoton transitions while in the strong field limit, for $\gamma \ll 1$, tunnel ionization takes place. In this latter case, the electron can escape from the vicinity of the ion core by tunneling through the barrier formed by the Coulomb attraction of the core and the time-dependent electric field generated by the laser. Once the electron is released, it is driven back and forth by the external field. It can therefore experience multiple returns to the nucleus. When the electron gets back to the nucleus, it can be scattered by the ion core or recombine in the ground state of the atom leading to HOHG of the driving field [11–13]. This picture is the basis of a well-known theoretical model, the so-called "strong field approximation" (SFA) where it is assumed that the dynamics are governed by the coupling of the ground state with the continuum and that the ejected electron is described by a Volkov state that ignores the presence of the Coulomb potential.

In fact, for $\gamma \ll 1$ and *a fortiori* for $\gamma \approx 1$, it is impossible to make a clear-cut separation between the two mechanisms. Both of them, multiphoton processes and tunnel ionization play a role. This has been confirmed experimentally and by numerical simulations. High-resolution fully differential experimental data on single ionization of rare gases (He, Ne, and Ar) by short laser pulses have been obtained by Rudenko *et al.* [14]. Their data clearly show that deep in the tunneling regime, the low-energy ATI peaks exhibit a fine structure that is unambiguously attributed to a resonant multiphoton process. From the theoretical point of view, de Bohan [15] has shown that for $\gamma < 1$, the first ATI peaks corresponding to an electron energy smaller than twice the ponderomotive potential do not result from a tunneling process. This has been demonstrated by carefully analyzing the behavior of the ionized wave packet both in the momentum and configuration space. It is important to note that it is precisely the low-energy part of the ATI spectrum that provides the dominant contribution to the ionization yield for a given photon energy. These results raise the fundamental question of the actual role of the Coulomb potential in the intensity regime where tunnel ionization is supposed to take place. In order to address this question, we have developed a model calculation which goes far beyond the SFA. It is this mathematical model that we present in this contribution.

de Bohan [15] has shown that in the present context it is more "natural" to solve the TDSE in the momentum space. By using Ehrenfest's theorem, it is easy to show that in the velocity gauge, the canonical momentum of continuum

*hugues.tetchou@uclouvain.be
†bernard.piraux@uclouvain.be

electrons becomes a constant of motion which, in atomic units, is equal to the electron drift velocity. As a result, working in the momentum space, provides direct informations on the ionization dynamics and in particular on the time at which the electron is emitted. In our model, we start from the TDSE associated with the interaction (in the velocity gauge) of atomic hydrogen with an intense infrared field. The external electric field is supposed to be linearly polarized. In the momentum space, the Coulomb potential is nonlocal. The main idea of the present approach is to substitute the kernel of the nonlocal Coulomb potential by a sum of N separable potentials, each of them supporting one bound state of atomic hydrogen. This approach which is widely used in nuclear physics for short-range potentials, allows one to reduce the three-dimensional TDSE to a system of N coupled one-dimensional linear Volterra integral equations of the second kind that we solve numerically. The present model presents several advantages. First, it provides a rigorous solution for the electron wave packet. Second, and by contrast with the SFA, more than one bound state may be included in the model, third, the continuum-continuum dipole matrix elements are treated exactly, and finally, the theory is fully gauge invariant.

This contribution is organized as follows. In the second section, we give a general formulation of the problem. In the next section, we show how to construct the separable potentials. In the fourth section, we describe our theoretical treatment of the TDSE in momentum space. We consider separately the case where the first two s states are included and the case where the $1s$, $2s$, and $2p$ are taken into account. The calculation of various observables at the end of the interaction with the pulse, in particular, the ionization yield and the electron energy spectrum, is given in the fifth section. In the sixth section, we discuss the numerical implementation of the method used to solve the linear Volterra integral equations of the second kind. Finally, before the conclusions, and in order to validate our model we consider in section seven, various physical situations in which the dynamics is well known. Unless stated, we use atomic units throughout this paper.

II. GENERAL FORMULATION

In the momentum space, the TDSE that governs the dynamics of atomic hydrogen exposed to a laser field, linearly polarized along the unit vector $\vec{e}$, reads

$$\left[\mathrm{i}\frac{\partial}{\partial t} - \frac{p^2}{2} - \frac{1}{c}A(t)(\vec{e}\cdot\vec{p})\right]\Phi(\vec{p},t) - \int \frac{d\vec{p}'}{(2\pi)^3}V(\vec{p},\vec{p}')\Phi(\vec{p}',t) = 0. \tag{1}$$

We work in the dipole approximation and use the velocity form for the laser-atom interaction Hamiltonian. c is the velocity of light and $A(t)$, the vector potential given by

$$A(t) = A_0 f(t)\sin(\omega t + \phi), \tag{2}$$

where A_0 is the vector potential amplitude, ϕ the carrier phase, ω the field frequency, and $f(t)$, the pulse envelope defined as follows:

$$f(t) = \begin{cases} \sin^2(\pi t/T), & 0 \leqslant t \leqslant T, \\ 0, & t > T, \end{cases} \tag{3}$$

with T, the total pulse duration. In terms of the laser peak intensity I, the amplitude A_0 of the vector potential is given by $(c/\omega)\sqrt{I/I_0}$ where the atomic unit of intensity $I_0 = 3.51 \times 10^{16}$ W/cm^2. It is important to note that if the total duration of the pulse is expressed as an integer number of optical periods T_p, there is no static electric field component. This prevents possible problems related to the gauge invariance [16]. The second term of the left-hand side of Eq. (1) is the Coulomb potential which, in the momentum space, is not local. The kernel $V(\vec{p},\vec{p}')$ is given by

$$V(\vec{p},\vec{p}') = -\frac{4\pi Z}{|\vec{p}-\vec{p}'|^2}, \tag{4}$$

where Z is the nucleus charge. Our model consists in replacing this kernel by a sum of separable potentials, each of them supporting one bound state of atomic hydrogen. The derivation of these separable potentials is explained in the following section.

III. CALCULATION OF THE SEPARABLE POTENTIALS

We write the kernel $V(\vec{p},\vec{p}')$ of the nonlocal Coulomb potential as a sum of N symmetric separable potentials [17]:

$$V(\vec{p},\vec{p}') = -\sum_{n=1}^{N} v_n(\vec{p})v_n^*(\vec{p}'). \tag{5}$$

We demand that this new kernel supports N atomic hydrogen bound eigenstates $|\varphi_n\rangle$ of eigenenergy ε_n. This means that

$$\left(\varepsilon_j - \frac{1}{2}p^2\right)\varphi_j(\vec{p}) + \sum_{n=1}^{N} a_{jn}v_n(\vec{p}) = 0, \tag{6}$$

where

$$a_{jn} = \int \frac{d\vec{p}'}{(2\pi)^3}v_n^*(\vec{p}')\varphi_j(\vec{p}'). \tag{7}$$

The coefficients a_{jn} are the elements of an $N \times N$ matrix $\mathbf{A}$. Let us define the vector $\mathbf{V}$ consisting of the elements $\{v_n(\vec{p})\}$, and the vector Φ consisting of the elements $\{(\varepsilon_j - \frac{1}{2}p^2)\varphi_j(\vec{p})\}$. In these notations, Eq. (6) writes

$$\Phi = -\mathbf{A}\mathbf{V}, \tag{8}$$

or, provided that $\mathbf{A}^{-1}$ exists,

$$\mathbf{V} = -\mathbf{A}^{-1}\Phi. \tag{9}$$

We now introduce the symmetric $N \times N$ matrix $\mathbf{\Gamma}$ defined by

$$\mathbf{\Gamma} = \mathbf{A}\mathbf{A}^{\mathbf{T}}, \tag{10}$$

where $\mathbf{A}^{\mathbf{T}}$ denotes the transpose matrix of $\mathbf{A}$. The elements of $\mathbf{\Gamma}$ are given by

$$\gamma_{ij} = -\int \frac{d\vec{p}}{(2\pi)^3}\varphi_i^*(\vec{p})\left(\varepsilon_j - \frac{1}{2}p^2\right)\varphi_j(\vec{p}) = \int \frac{d\vec{r}}{r}\tilde{\varphi}_i^*(\vec{r})\tilde{\varphi}_j(\vec{r}). \tag{11}$$

This is a general scheme for the factorization of the Coulomb potential. The integrals in (11) are well known. They only

allow transitions $ns \to ms$,$np \to mp$,$nd \to md$, and so on. In addition, it is clear that the matrix $\mathbf{\Gamma}$ is block diagonal, each l-block being associated with the value of the angular momentum l. This and the angular structure of the hydrogen eigenfunctions,

$$\varphi_{nlm}(\vec{p}) = R_{nl}(p)Y_{lm}(\vec{p}), \quad l \leqslant n-1, \tag{12}$$

allow one to rewrite the separable potential in the following way:

$$V(\vec{p},\vec{p}') = -V^{(s)}(\vec{p},\vec{p}') - V^{(p)}(\vec{p},\vec{p}') - V^{(d)}(\vec{p},\vec{p}') - \cdots, \tag{13}$$

with

$$V^{(l)}(\vec{p},\vec{p}') = \sum_{j=1}^{N_l} v_j^{(l)}(p)v_j^{(l)}(p')\langle Y_l(\vec{p})\cdot Y_l(\vec{p}')\rangle, \tag{14}$$

where $\langle Y_l(\vec{p})\cdot Y_l(\vec{p}')\rangle$ is the scalar product of spherical harmonics, and N_l is an integer denoting the number of angular momentum among the N atomic bound energies considered in Eq. (5). As a result, Eq. (6) takes the form:

$$\left(\varepsilon_j - \frac{1}{2}p^2\right) R_{jl}(p) + \sum_{j'=1}^{N_l} a_{jj'}^{(l)} v_{j'}^{(l)}(p) = 0, \tag{15}$$

where

$$a_{jj'}^{(l)} = \int_0^\infty \frac{p^2 dp}{(2\pi)^3} R_{jl}(p)v_{j'}^{(l)}(p), \tag{16}$$

and determines the form of the potential functions inside an l-block.

According to Eq. (9), we have to solve a system of algebraic equations for each l-block. Its solution, however, is not unique. In the case of hydrogen atom $Z = 1$, let us consider for instance, the $(1s + 2s)$ potential whose components are given by

$$\begin{aligned} v_1^{(s)}(p) &= \alpha_{11}\left(\varepsilon_1 - \tfrac{1}{2}p^2\right) R_{1s}(p) + \alpha_{12}\left(\varepsilon_2 - \tfrac{1}{2}p^2\right) R_{2s}(p), \\ v_2^{(s)}(p) &= \alpha_{21}\left(\varepsilon_1 - \tfrac{1}{2}p^2\right) R_{1s}(p) + \alpha_{22}\left(\varepsilon_2 - \tfrac{1}{2}p^2\right) R_{2s}(p), \end{aligned} \tag{17}$$

with

$$\begin{aligned} R_{1s}(p) &= \frac{16\pi}{(p^2+1)^2}, \quad \varepsilon_1 = -1/2, \\ R_{2s}(p) &= 4\sqrt{2}\pi\,\frac{(p^2-1/4)}{(p^2+1/4)^3}, \quad \varepsilon_2 = -1/8. \end{aligned} \tag{18}$$

From Eq. (10), we obtain the following system of nonlinear equations:

$$\begin{aligned} a_{11}^2 + a_{12}^2 = \gamma_{11}, \quad a_{21}^2 + a_{22}^2 = \gamma_{22}, \\ a_{11}a_{21} + a_{22}a_{12} = \gamma_{12}, \end{aligned} \tag{19}$$

where

$$\gamma_{11} = 1, \quad \gamma_{22} = \frac{1}{4}, \quad \gamma_{12} = \frac{4\sqrt{2}}{27}. \tag{20}$$

The general solution takes the form,

$$\begin{aligned} \alpha_{11} &= -\frac{\cos(\kappa-\theta)}{\sqrt{\gamma_{11}}\cos\kappa}, \quad \alpha_{12} = \frac{\sin\theta}{\sqrt{\gamma_{22}}\cos\kappa}, \\ \alpha_{21} &= \frac{\sin(\kappa-\theta)}{\sqrt{\gamma_{11}}\cos\kappa}, \quad \alpha_{22} = -\frac{\cos\theta}{\sqrt{\gamma_{22}}\cos\kappa}, \end{aligned} \tag{21}$$

where θ is an arbitrary angle and κ can take two possible values: $\kappa_1 = \arcsin(\gamma_{12}/\sqrt{\gamma_{11}\gamma_{22}})$ and $\kappa_2 = \pi - \arcsin(\gamma_{12}/\sqrt{\gamma_{11}\gamma_{22}})$. Hence, we clearly see that there are two families of solutions characterized by the two pairs of parameters (κ_1,θ) and (κ_2,θ). Therefore, it is necessary to determine some rules to select the unique potential. We can, for instance, force the l-blocks of matrix $\mathbf{A}^{-1}$ to be triangular. This particular choice fixes the value of θ to zero in Eq. (21). In that case, $\alpha_{11} = -1/\sqrt{\gamma_{11}}$ and $\alpha_{12} = 0$. In turn, $\alpha_{21} = \tan\kappa_1/\sqrt{\gamma}_{11}$ and $\alpha_{22} = -1/(\sqrt{\gamma_{22}}\cos\kappa_1)$. Note that if instead of κ_1 we use κ_2, both coefficients α_{21} and α_{22} change their sign. This, however, has no impact because it is only the products $v_j^{(l)}(p)v_j^{(l)}(p')$ that enter the separable potentials. Instead of imposing a triangular structure to the matrix $\mathbf{A}^{-1}$, we could equally well force this matrix to be symmetric which implies that $\alpha_{12} = \alpha_{21}$ in Eq. (21). Such a rule, however, does not lead to a unique solution. This ambiguity is well known from nuclear physics and has been discussed by Bargmann [18] and Weinberg [19]. In the present case, we assume matrix $\mathbf{A}^{-1}$ symmetric and write

$$\tan\theta = \frac{\sin\kappa}{(\sqrt{\gamma_{11}/\gamma_{22}} + \cos\kappa)},$$

with $\kappa = \kappa_2$. Note that if we choose the l-blocks of matrix $\mathbf{A}^{-1}$ to be triangular or $\kappa = \kappa_1$ in the last expression of $\tan\theta$, the potential components $v_j^{(l)}(p)$ have not always the same sign. In that case, the corresponding separable potential (5) may be positive (repulsive) in contrast to the kernel (4) associated with the Coulomb potential. On the other hand it is important to stress that irrespective of the choice of the separable potentials, the wave function associated with the atomic hydrogen bound state that these separable potentials support is exact. Therefore the previous discussion shows that the unphysical effects we observe in our final results with the wrong choice of the separable potentials are linked to a very bad description of the continuum wave functions. When our model atom contains only the ground state, it is needless to say that the previous argumentation about the choice of a separable potential is irrelevant. This particular case has been treated in [17,20].

IV. SOLUTION OF THE TDSE IN MOMENTUM SPACE

A. $(1s + 2s)$ model potential

According to the previous scheme, the TDSE for the "$(1s + 2s)$ hydrogenlike atom" writes, in momentum space, as follows:

$$\begin{aligned} &\left[\mathrm{i}\frac{\partial}{\partial t} - \frac{p^2}{2} + (\vec{e}\cdot\vec{p})\left(\frac{\partial}{\partial t}b(t)\right)\right]\Phi(\vec{p},t) \\ &\quad + v_1^{(s)}(p)Y_{00}(\vec{p})F_1(t) + v_2^{(s)}(p)Y_{00}(\vec{p})F_2(t) = 0, \end{aligned} \tag{22}$$

where

$$F_j(t) = \int \frac{d\vec{p}}{(2\pi)^3}\, v_j^{(s)}(p) Y_{00}^*(\vec{p}) \Phi(\vec{p},t); \quad j = 1,2. \quad (23)$$

The initial condition is $\Phi(\vec{p},0) = \varphi_{1s}(\vec{p})$ and we use for convenience $b(t) = -(1/c)\int_0^t A(\tau)\, d\tau$. Equation (22) can be solved formally. Its solution which satisfies the initial condition reads

$$\Phi(\vec{p},t) = \exp\left[-it p^2/2 + ib(t)(\vec{e}\cdot\vec{p})\right]\Bigg[\varphi_{1s}(\vec{p}) + i\int_0^t d\xi \times \left[v_1^{(s)}(p) Y_{00}(\vec{p}) F_1(\xi) + v_2^{(s)}(p) Y_{00}(\vec{p}) F_2(\xi)\right] \times \exp\left[i\xi p^2/2 - ib(\xi)(\vec{e}\cdot\vec{p})\right]\Bigg]. \quad (24)$$

If we define

$$J_{\mu\nu}(x,y) = \frac{1}{2(2\pi)^3 \mathrm{i} y}\int_{-\infty}^{\infty} p\, R_{\mu s}(p) R_{\nu s}(p) \exp(-ixp^2 + iyp)\, dp \quad (\mu,\nu = 1,2), \quad J_{\mu\nu}(0,0) = \delta_{\mu\nu}, \quad (25)$$

we obtain from Eqs. (23) and (24), a system of time-dependent linear Volterra integral equations which can be written in matrix form as follows:

$$\mathbf{F}(t) = \mathbf{F}_0(t) + \int_0^t \mathbf{K}(t,\xi)\mathbf{F}(\xi)\, d\xi. \quad (26)$$

The elements of vector $\mathbf{F}_0(t)$ are given by

$$F_{10}(t) = \left[\alpha_{11}\left(\varepsilon_1 - \frac{\mathrm{i}}{2}\frac{\partial}{\partial x}\right) J_{11}(x,b(t)) + \alpha_{12}\left(\varepsilon_2 - \frac{i}{2}\frac{\partial}{\partial x}\right) J_{12}(x,b(t))\right]_{x=t/2},$$
$$F_{20}(t) = \left[\alpha_{21}\left(\varepsilon_1 - \frac{\mathrm{i}}{2}\frac{\partial}{\partial x}\right) J_{11}(x,b(t)) + \alpha_{22}\left(\varepsilon_2 - \frac{i}{2}\frac{\partial}{\partial x}\right) J_{12}(x,b(t))\right]_{x=t/2}. \quad (27)$$

The elements of the 2×2 matrix $\mathbf{K}$ are

$$K_{11}(t,\xi) = i\left[\alpha_{11}^2\left(\varepsilon_1 - \frac{i}{2}\frac{\partial}{\partial x}\right)^2 J_{11}(x,y) + 2\alpha_{11}\alpha_{12}\left(\varepsilon_1 - \frac{i}{2}\frac{\partial}{\partial x}\right)\left(\varepsilon_2 - \frac{i}{2}\frac{\partial}{\partial x}\right) J_{12}(x,y) + \alpha_{12}^2\left(\varepsilon_2 - \frac{i}{2}\frac{\partial}{\partial x}\right)^2 J_{22}(x,y)\right]_{x=(t-\xi)/2,\ y=b(t)-b(\xi)},$$

$$K_{12}(t,\xi) = K_{21}(t,\xi) = i\left[\alpha_{11}\alpha_{21}\left(\varepsilon_1 - \frac{i}{2}\frac{\partial}{\partial x}\right)^2 J_{11}(x,y) + (\alpha_{11}\alpha_{22} + \alpha_{21}\alpha_{12})\left(\varepsilon_1 - \frac{i}{2}\frac{\partial}{\partial x}\right)\left(\varepsilon_2 - \frac{i}{2}\frac{\partial}{\partial x}\right) J_{12}(x,y) + \alpha_{12}\alpha_{22}\left(\varepsilon_2 - \frac{i}{2}\frac{\partial}{\partial x}\right)^2 J_{22}(x,y)\right]_{x=(t-\xi)/2,\ y=b(t)-b(\xi)}, \quad (28)$$

$$K_{22}(t,\xi) = i\left[\alpha_{21}^2\left(\varepsilon_1 - \frac{i}{2}\frac{\partial}{\partial x}\right)^2 J_{11}(x,y) + 2\alpha_{21}\alpha_{22}\left(\varepsilon_1 - \frac{i}{2}\frac{\partial}{\partial x}\right)\left(\varepsilon_2 - \frac{i}{2}\frac{\partial}{\partial x}\right) J_{12}(x,y) + \alpha_{22}^2\left(\varepsilon_2 - \frac{i}{2}\frac{\partial}{\partial x}\right)^2 J_{22}(x,y)\right]_{x=(t-\xi)/2,\ y=b(t)-b(\xi)}.$$

From Eqs. (25)–(28), we easily obtain an expression of the amplitude of probability for the system to be in one of the two bound states ($1s$ or $2s$) as a function of time:

$$C_{1s}(t) = \langle\varphi_{1s}|\Phi(t)\rangle = J_{11}[t/2,b(t)] + i\int_0^t d\xi\ F_1(\xi)\left[\alpha_{11}\left(\varepsilon_1 - \frac{i}{2}\frac{\partial}{\partial x}\right) J_{11}(x,y) + \alpha_{12}\left(\varepsilon_2 - \frac{i}{2}\frac{\partial}{\partial x}\right) J_{12}(x,y)\right]_{x=(t-\xi)/2,\ y=b(t)-b(\xi)} + i\int_0^t d\xi\ F_2(\xi)\left[\alpha_{21}\left(\varepsilon_1 - \frac{i}{2}\frac{\partial}{\partial x}\right) J_{11}(x,y) + \alpha_{22}\left(\varepsilon_2 - \frac{i}{2}\frac{\partial}{\partial x}\right) J_{12}(x,y)\right]_{x=(t-\xi)/2,\ y=b(t)-b(\xi)},$$

$$C_{2s}(t) = \langle\varphi_{2s}|\Phi(t)\rangle = J_{12}[t/2,b(t)] + i\int_0^t d\xi\, F_1(\xi)\left[\alpha_{11}\left(\varepsilon_1 - \frac{i}{2}\frac{\partial}{\partial x}\right) J_{12}(x,y) + \alpha_{12}\left(\varepsilon_2 - \frac{i}{2}\frac{\partial}{\partial x}\right) J_{22}(x,y)\right]_{x=(t-\xi)/2,\ y=b(t)-b(\xi)} + i\int_0^t d\xi\ F_2(\xi)\left[\alpha_{21}\left(\varepsilon_1 - \frac{i}{2}\frac{\partial}{\partial x}\right) J_{12}(x,y) + \alpha_{22}\left(\varepsilon_2 - \frac{i}{2}\frac{\partial}{\partial x}\right) J_{22}(x,y)\right]_{x=(t-\xi)/2,\ y=b(t)-b(\xi)}. \quad (29)$$

B. $(1s + 2s + 2p)$ model potential

Let us now introduce the $2p$ component of the separable potential in the TDSE. In momentum space, the wave function of the $2p$ state is given by

$$\varphi_{2pm}(\vec{p}) = R_{2p}(p)\, Y_{1m}(\vec{p}) = \frac{8\pi}{\sqrt{6}}\, \frac{p}{(p^2+1/4)^3}\, Y_{1m}(\vec{p}). \quad (30)$$

By using the same rule as before, we obtain for the $2p$ component of the separable potential, the following expression:

$$v_1^{(p)}(p) = \frac{\sqrt{8\pi}\, p}{(p^2+1/4)^2}. \quad (31)$$

In this condition, the TDSE becomes

$$\left[\mathrm{i}\frac{\partial}{\partial t} - \frac{p^2}{2} + (\vec{e}\cdot\vec{p})\left(\frac{\partial}{\partial t} b(t)\right)\right]\Phi(\vec{p},t) + v_1^{(s)}(p) Y_{00}(\vec{p}) F_1(t)$$
$$+ v_2^{(s)}(p) Y_{00}(\vec{p}) F_2(t) + v_1^{(p)}(p) \sum_{m=-1}^{1} Y_{1m}(\vec{p}) F_{3m}(t) = 0, \quad (32)$$

where

$$F_{3m}(t) = \int \frac{d\vec{p}}{(2\pi)^3}\, v_1^{(p)}(p) Y_{1m}^*(\vec{p}) \Phi(\vec{p},t). \quad (33)$$

Given the symmetry of the problem, we can write $F_{3m}(t) = F_3(t) Y_{1m}^*(\vec{e})$. This means that

$$F_3(t) = \int \frac{d\vec{p}}{(2\pi)^3 p}\, v_1^{(p)}(p)(\vec{e}\cdot\vec{p})\Phi(\vec{p},t), \quad (34)$$

and

$$\sum_{m=-1}^{1} Y_{1m}(\vec{p}) F_{3m}(t) = \frac{3}{4\pi}\frac{(\vec{e}\cdot\vec{p})}{p} F_3(t). \quad (35)$$

Consequently, the solution of Eq. (32) takes the following form:

$$\Phi(\vec{p},t) = \exp\left[-it\,p^2/2 + ib(t)(\vec{e}\cdot\vec{p})\right]$$
$$\times\left[\varphi_{1s}(\vec{p}) + i\int_0^t d\xi\left(v_1^{(s)}(p) Y_{00}(\vec{p}) F_1(\xi)\right.\right.$$
$$\left.\left. + v_2^{(s)}(p) Y_{00}(\vec{p}) F_2(\xi) + \frac{3}{4\pi} v_1^{(p)}(p)\frac{(\vec{e}\cdot\vec{p})}{p} F_3(\xi)\right)\right.$$
$$\left.\times \exp\left[i\xi\, p^2/2 - i b(\xi)(\vec{e}\cdot\vec{p})\right]\right]. \quad (36)$$

As in the previous case, the functions F_j with $j = 1,2,3$ are the solution of a system of three coupled time-dependent linear Volterra integral equations which can be written in matrix form as follows:

$$\mathbf{F}(t) = \mathbf{F}_0(t) + \int_0^t \mathbf{K}(t,\xi)\mathbf{F}(\xi)\, d\xi. \quad (37)$$

The new 3×3 matrix $\mathbf{K}$ includes three new elements:

$$K_{j3}(t,\xi) = K_{3j}(t,\xi) = i\int \frac{d\vec{p}}{(2\pi)^3 p}\, v_j^{(s)}(p) Y_{00}^*(\vec{p}) v_1^{(p)}(p)$$
$$\times (\vec{e}\cdot\vec{p})\exp\{-i(t-\xi)p^2/2$$
$$+ i[b(t) - b(\xi)](\vec{e}\cdot\vec{p})\}, \quad j = 1,2, \quad (38)$$

$$K_{33}(t,\xi) = i\frac{3}{4\pi}\int \frac{d\vec{p}}{(2\pi)^3 p^2}\left[v_1^{(p)}(p)\right]^2 (\vec{e}\cdot\vec{p})^2$$
$$\times \exp\{-i(t-\xi)p^2/2 + i[b(t) - b(\xi)](\vec{e}\cdot\vec{p})\}.$$

The third element of $\mathbf{F}_0(t)$ is given by

$$F_{30}(t) = \int \frac{d\vec{p}}{(2\pi)^3 p}\, \varphi_{1s}(\vec{p}) v_1^{(p)}(p)(\vec{e}\cdot\vec{p})$$
$$\times \exp\left[-it\,p^2/2 + ib(t)(\vec{e}\cdot\vec{p})\right]. \quad (39)$$

As before, we introduce three new functions similar to those defined by Eq. (25):

$$J_{k3}(x,y) = \frac{\sqrt{3}}{2(2\pi)^3 iy}\int_{-\infty}^{\infty} R_{ks}(p) R_{2p}(p)$$
$$\times \exp\left(-ixp^2 + iyp\right) dp, \quad k = 1,2, \quad (40)$$
$$J_{33}(x,y) = \frac{6}{(2\pi)^3 iy}\int_{-\infty}^{\infty} R_{2p}^2(p)\exp\left(-ixp^2 + iyp\right)\frac{dp}{p}.$$

In terms of these functions, the three new elements of matrix $\mathbf{K}$ write:

$$K_{13}(t,\xi) = -\frac{\partial}{\partial y}\left(\varepsilon_2 - \frac{i}{2}\frac{\partial}{\partial x}\right)\left[\alpha_{11}\left(\varepsilon_1 - \frac{i}{2}\frac{\partial}{\partial x}\right) J_{13}(x,y)\right.$$
$$\left. + \alpha_{12}\left(\varepsilon_2 - \frac{i}{2}\frac{\partial}{\partial x}\right) J_{23}(x,y)\right],$$

$$K_{23}(t,\xi) = -\frac{\partial}{\partial y}\left(\varepsilon_2 - \frac{i}{2}\frac{\partial}{\partial x}\right)\left[\alpha_{21}\left(\varepsilon_1 - \frac{i}{2}\frac{\partial}{\partial x}\right) J_{13}(x,y)\right.$$
$$\left. + \alpha_{22}\left(\varepsilon_2 - \frac{i}{2}\frac{\partial}{\partial x}\right) J_{23}(x,y)\right],$$

$$K_{33}(t,\xi) = -i\frac{3}{4\pi}\frac{\partial^2}{\partial y^2}\left(\varepsilon_2 - \frac{i}{2}\frac{\partial}{\partial x}\right)^2 J_{33}(x,y), \quad (41)$$

where $x = (t-\xi)/2$, $y = b(t) - b(\xi)$ after performing all differentiations. Similarly, we have

$$F_{30}(t) = i\left[\frac{\partial}{\partial y}\left(\varepsilon_2 - \frac{i}{2}\frac{\partial}{\partial x}\right) J_{13}(x,y)\right]_{x=t/2,\ y=b(t)}. \quad (42)$$

Let us now calculate the population of the $2p$ state. The corresponding amplitude reads

$$C_{2p,m}(t) = \langle\varphi_{2pm}|\Phi(t)\rangle. \quad (43)$$

As before, the symmetry of the problem allows us to write $C_{2p,m}(t) = C_{2p}(t) Y_{1m}(\vec{e})$ with

$$C_{2p}(t) = \int \frac{d\vec{p}}{(2\pi)^3}\frac{(\vec{e}\cdot\vec{p})}{p} R_{2p}(p)\Phi(\vec{p},t)$$
$$= -i\sqrt{\frac{\pi}{3}}\left[\frac{\partial}{\partial y} J_{13}(t/2,y)\right]_{y=b(t)} + \sqrt{\frac{\pi}{3}}\int_0^t d\xi\ F_1(\xi)$$
$$\times\left[\alpha_{11}\left(\varepsilon_1 - \frac{i}{2}\frac{\partial}{\partial x}\right)\frac{\partial}{\partial y} J_{13}(x,y)\right.$$
$$\left. + \alpha_{12}\left(\varepsilon_2 - \frac{i}{2}\frac{\partial}{\partial x}\right)\frac{\partial}{\partial y} J_{23}(x,y)\right]_{x=(t-\xi)/2,\ y=b(t)-b(\xi)}$$
$$+ \sqrt{\frac{\pi}{3}}\int_0^t d\xi\ F_2(\xi)\left[\alpha_{21}\left(\varepsilon_1 - \frac{i}{2}\frac{\partial}{\partial x}\right)\frac{\partial}{\partial y} J_{13}(x,y)\right.$$

$$+\alpha_{22}\left(\varepsilon_2-\frac{i}{2}\frac{\partial}{\partial x}\right)\frac{\partial}{\partial y}J_{23}(x,y)\Bigg]_{x=(t-\xi)/2,\ y=b(t)-b(\xi)}$$
$$+i\sqrt{\frac{3}{16\pi}}\int_0^t d\xi\ F_3(\xi)$$
$$\times\left[\left(\varepsilon_2-\frac{i}{2}\frac{\partial}{\partial x}\right)\frac{\partial^2}{\partial y^2}J_{33}(x,y)\right]_{x=(t-\xi)/2,\ y=b(t)-b(\xi)}. \tag{44}$$

Furthermore, we have

$$\sum_{m=-1}^{1}|C_{2p,m}(t)|^2=\frac{3}{4\pi}|C_{2p}(t)|^2. \tag{45}$$

It is clear that the amplitudes C_{1s} and C_{2s} must be calculated with the new wave packet (36). This leads to adding new terms in (29), which include the integrals in $F_3(\xi)$ and the corresponding derivatives of the functions J_{j3}, $j=1,2$. Incidentally, our separable (nonlocal) potential can possibly have more bound states than the selected amount. In this case, it is necessary to determine all bound states beforehand. This is done by setting in Eq. (32), $b(t)=0$ and $|\Phi(t)\rangle=e^{-i\varepsilon_s t}|\varphi_s\rangle$ ($\varepsilon_s<0$), and by solving the system of algebraic equations for the values $f_j=e^{i\varepsilon_s t}F_j(t)$.

In the momentum space, it is rather subtle to formulate the gauge invariance of Eq. (22) or (32). Instead, it is more convenient to go back momentarily to the configuration space. As it is in momentum space, each component of the atomic potential is nonlocal and separable. It therefore involves a product of functions $\tilde{v}(\vec{r})\tilde{v}^*(\vec{r}')$. Within the dipole approximation, the unitary transformation that allows one to move from the velocity to the length gauge must be applied to both the functions $\tilde{v}(\vec{r})$ and $\tilde{v}^*(\vec{r}')$ to guarantee the gauge invariance.

C. Methodological aspects

We show in the appendix that all basic functions $J_{\mu\nu}$ are expressed in terms of an analytical function denoted by $I(x,y,\gamma)$ and its derivatives. In this section, we define and analyze the properties of the successive derivatives of this function. We first introduce the following expressions:

$$R_\pm\equiv R(x,\pm y;\gamma)=\exp(\pm y\sqrt{\gamma})\,\mathrm{erfc}\Bigg(\exp(i\pi/4)\sqrt{x\gamma}$$
$$\pm\exp(-i\pi/4)\frac{y}{2\sqrt{x}}\Bigg), \tag{46}$$

where

$$\mathrm{erfc}(z)=1-\frac{2}{\sqrt{\pi}}\int_0^z\exp(-\xi^2)\,d\xi, \tag{47}$$

is the complementary error function [21]. We now define the function $I(x,y;\gamma)$ as follows:

$$I(x,y;\gamma)=\frac{i\pi}{2}\exp(ix\gamma)[R_- - R_+]. \tag{48}$$

The basic integrals entering the calculation of the kernels may be expressed in terms of the derivatives of this function $I(x,y,\gamma)$ with respect to γ:

$$\int_{-\infty}^{\infty}\frac{p\,dp}{(p^2+\gamma)^{n+1}}\exp(-ixp^2+iyp)$$
$$=(-1)^n\frac{1}{n!}\frac{\partial^n}{\partial\gamma^n}I(x,y;\gamma), \tag{49}$$

$$\int_{-\infty}^{\infty}\frac{p\,dp}{(p^2+\gamma)^{n+1}(p^2+\beta)^{m+1}}\exp(-ixp^2+iyp)$$
$$=\frac{(-1)^{n+m}}{n!m!}\frac{\partial^{n+m}}{\partial\gamma^n\partial\beta^m}\frac{1}{(\beta-\gamma)}[I(x,y;\gamma)-I(x,y;\beta)]. \tag{50}$$

Taking into account the following equation,

$$\frac{\partial R_\pm}{\partial\gamma}=\pm\frac{y}{2\sqrt{\gamma}}\,R_\pm-\sqrt{\frac{x}{\pi\gamma}}\,\exp[i(\pi/4-x\gamma+y^2/4x)], \tag{51}$$

it is straightforward to show that

$$\frac{\partial I}{\partial\gamma}=ixI-\frac{i\pi y}{4\sqrt{\gamma}}\,\exp(ix\gamma)\,[R_-+R_+], \tag{52}$$

$$\frac{\partial^2 I}{\partial\gamma^2}=\left(2ix-\frac{1}{2\gamma}\right)\frac{\partial I}{\partial\gamma}+\left(x^2+\frac{ix}{2\gamma}+\frac{y^2}{4\gamma}\right)I$$
$$+\frac{y\sqrt{\pi x}}{2\gamma}\,\exp[i(3\pi/4+y^2/2x)], \tag{53}$$

and to generalize these results to the $(n+1)$th derivative of I. We obtain

$$\frac{\partial^{n+1}I}{\partial\gamma^{n+1}}=a_n\,\frac{\partial I}{\partial\gamma}+b_n\,I+c_n, \tag{54}$$

with

$$a_{n+1}=a_n a_1+\frac{\partial a_n}{\partial\gamma}+b_n,\quad b_{n+1}=a_n b_1+\frac{\partial b_n}{\partial\gamma},$$
$$c_{n+1}=a_n c_1+\frac{\partial c_n}{\partial\gamma},\quad n=1,2,\ldots, \tag{55}$$

and

$$a_1=\left(2ix-\frac{1}{2\gamma}\right),\quad b_1=\left(x^2+\frac{ix}{2\gamma}+\frac{y^2}{4\gamma}\right),$$
$$c_1=\frac{y\sqrt{\pi x}}{2\gamma}\,\exp[i(3\pi/4+y^2/2x)]. \tag{56}$$

It is interesting to mention the following inequality:

$$\left|\frac{\partial^n}{\partial\gamma^n}I(x,y;\gamma)\right|\leqslant 2n!\int_0^\infty\frac{p\,dp}{(p^2+\gamma)^{n+1}}$$
$$=\frac{(n-1)!}{\gamma^n},\quad n\geqslant 1, \tag{57}$$

which is valid for any values of the variables x and y. Equation (57) shows that already the first derivative of I with respect to the parameter γ is bounded and has no singularities. In the appendix, we give the expression of $J_{\mu\nu}$ in terms of

the derivatives of $I(x,y;\gamma)$ with respect to the parameter γ. Clearly, these expressions are free of singularities and have a behavior that does not raise any numerical difficulty. In fact, from the numerical point of view, the most problematic is the behavior of the ratio I/y and its derivatives with respect to y. From Eq. (48), we obtain the following limit:

$$\lim_{y\to 0}\frac{I(x,y;\gamma)}{2iy}=\frac{1}{2}\exp(-i\pi/4)\sqrt{\frac{\pi}{x}}-\frac{\pi\sqrt{\gamma}}{2}\times\exp(ix\gamma)\,\mathrm{erfc}[\exp(i\pi/4)\sqrt{\gamma x}]. \quad (58)$$

This expression is singular for $x\to 0$, but this singular term does not depend on γ and disappears after differentiating with respect to this parameter. So, if we have to differentiate the ratio I/y with respect to γ, the first singular term can be simply omitted when $x\to 0$.

Let us now investigate how to perform the derivatives with respect to y in Eqs. (41)–(44). It is useful in that case to introduce the following integral [22]:

$$B(x,y;\gamma)=\int_0^\infty\frac{dp}{(p^2+\gamma)}\exp(-ixp^2)\cos yp=\frac{\pi}{4\sqrt{\gamma}}\exp(ix\gamma)[R_-+R_+]. \quad (59)$$

From Eqs. (49) and (52), we can write

$$I(x,y;\gamma)=-2i\frac{\partial B}{\partial y},\quad \frac{\partial I}{\partial\gamma}=ixI-iyB.$$

Given the indefinite integral [22],

$$\int dx\exp\left(-a^2x^2-\frac{b^2}{x^2}\right)=\frac{\sqrt{\pi}}{4a}\left[\exp(2ab)\,\mathrm{erf}\left(ax+\frac{b}{x}\right)+\exp(-2ab)\,\mathrm{erf}\left(ax-\frac{b}{x}\right)\right]+\mathrm{const}, \quad (60)$$

we can rewrite the function $B(x,y;\gamma)$ in the following form:

$$B(x,y;\gamma)=\frac{\sqrt{\pi}}{2}\exp(ix\gamma+i\pi/4)\int_x^\infty\frac{d\xi}{\sqrt{\xi}}\exp(-i\xi\gamma+iy^2/4\xi). \quad (61)$$

A simple change of variable in (60) namely $\xi=x(\eta+1)$ gives another useful representation:

$$B(x,\zeta;\gamma)=\frac{\sqrt{\pi x}}{2}\exp(i\pi/4)\int_0^\infty\frac{d\eta}{\sqrt{\eta+1}}\times\exp\left(-ix\gamma\eta+\frac{i}{\eta+1}\zeta^2\right),\quad \zeta^2=y^2/4x. \quad (62)$$

The variable ζ in (62) is always finite because in all cases, it reduces to $b(t)/2\sqrt{t}$ or $|b(t)-b(\xi)|/2\sqrt{t-\xi}$. The integral is of the order of $x^{-1/2}$ when $x\to 0$, but this behavior is compensated by $\sqrt{x}$ before the integral so that $B(0,\zeta;\gamma)$ exists and is finite. We are now ready to calculate:

$$\frac{\partial^s}{\partial\gamma^s}\frac{\partial^2}{\partial y^2}\left(\frac{I}{y}\right)=\frac{\sqrt{\pi}}{2}\exp[i(\pi/4-\pi s/2)]x^{s-3/2}\times\left[\frac{i}{2}g_{s,2}(x,\zeta)-\zeta^2 g_{s,3}(x,\zeta)\right], \quad (63)$$

where by definition,

$$g_{s,\mu}(x,\zeta)=\int_0^\infty\frac{\eta^s d\eta}{(\eta+1)^{\mu+1/2}}\exp\left(-ix\gamma\eta+\frac{i}{\eta+1}\zeta^2\right)=s!\sum_{n=0}^\infty\frac{(i\zeta^2)^n}{n!}\Psi(s+1,s-n-\mu+3/2;ix\gamma). \quad (64)$$

In Eq. (64), s,μ are integers, and Ψ is the confluent hypergeometric function with $\Psi(a,b;z)\sim z^{-a}$ for $z\to\infty$. Therefore, we have for large x,

$$g_{s,\mu}(x,\zeta)\approx\frac{s!}{(ix\gamma)^{s+1}}\exp(i\zeta^2). \quad (65)$$

Taking into account the prefactor in (62), we obtain $x^{s-3/2}g_{s,\mu}\sim x^{-5/2}$, and this asymptotic behavior does not depend either on s, or on μ. The limiting case $x\to 0$ is more delicate. Its investigation can be treated with the equation [21],

$$\Psi(a,b;z)=\frac{\Gamma(1-b)}{\Gamma(1+a-b)}\Phi(a,b;z)+z^{1-b}\frac{\Gamma(b-1)}{\Gamma(a)}\Phi(a-b+1,2-b;z), \quad (66)$$

which is always valid in our case ($0\leqslant s\leqslant 3,\ \mu=2,3$). Applying (66) to (64) and denoting z by $z=ix\gamma$, we obtain

$$\begin{aligned}&x^{s-3/2}\Psi(s+1,s-n-\mu+3/2;z)\\&=x^{s-3/2}\frac{\Gamma(n+\mu-s-1/2)}{\Gamma(n+\mu+1/2)}\Phi(s+1,s-n|,-\mu+3/2;z)\\&\quad+x^{n+\mu-2}(i\gamma)^{n+\mu-s-1/2}\frac{\Gamma(s-n-\mu+1/2)}{\Gamma(s+1)}\\&\quad\times\Phi(n+\mu+1/2,n+\mu-s+1/2;z).\end{aligned} \quad (67)$$

This expression is singular for $x\to 0$ when $s=0,1$. For $s=0$,

$$x^{-3/2}\Psi(1,-n-\mu+3/2;z)\approx\frac{x^{-3/2}}{n+\mu-1/2}-\frac{i\gamma x^{-1/2}}{(n+\mu-1/2)(n+\mu-3/2)}+O(1), \quad (68)$$

and for $s=1$,

$$x^{-1/2}\Psi(2,-n-\mu+5/2;z)\approx\frac{x^{-1/2}}{(n+\mu-1/2)(n+\mu-3/2)}+O(1). \quad (69)$$

In this case, the expression,

$$\begin{aligned}\mathcal{I}&=\frac{\partial^s}{\partial\gamma^s}\frac{\partial^2}{\partial y^2}\left(\frac{I(x,y;\gamma)-I(x,y;\beta)}{(\gamma-\beta)y}\right),\\&=\sum_{p=0}^s(-1)^{s-p}\frac{s!}{p!(\gamma-\beta)^{s-p+1}}\frac{\partial^p}{\partial\gamma^p}\frac{\partial^2}{\partial y^2}\\&\quad\times\left(\frac{I(x,y;\gamma)-I(x,y;\beta)}{y}\right),\end{aligned} \quad (70)$$

is not anymore singular at $x \to 0$. Furthermore, we can show that for $s \geqslant 1$,

$$\frac{\partial^s}{\partial\gamma^s}\frac{\partial^2}{\partial y^2}\left(\frac{I}{y}\right) = i^s \sum_{p=0}^{s} \frac{(-1)^p s!}{p!(s-p)!} x^{s-p} \times \left\{ \frac{i}{2}[\theta(2-p)A_{2-p} + \theta(p-2)G_{p-2}] , - \frac{y^2}{4}[\theta(3-p)A_{3-p} + \theta(p-3)G_{p-3}] \right\}, \quad (71)$$

is regular for $s \geqslant 2$. In this equation, $\theta(t)$ is the well-known Heaviside function, $G_m = (x + \mathrm{i}\frac{\partial}{\partial\gamma})^m B(x,y;\gamma)$ and $A_m = (\frac{-2\mathrm{i}}{y}\frac{\partial}{\partial y})^m B(x,y;\gamma)$. Note that the compensation of the singularity $x^{-1/2}$ is reached if we take into account the second term in Eq. (68) for $p = 0$ and for $p = 1$ in Eq. (69). As a result, the second derivative with respect to y takes the following form for $x \to 0$:

$$\frac{\partial^2}{\partial y^2}\left(\frac{I}{y}\right)_{x\to 0} \simeq x^{-3/2} f_1(\zeta^2) + x^{-1/2}\gamma f_2(\zeta^2) + O(1), \quad (72)$$

where both functions $f_1(\zeta^2)$ and $f_2(\zeta^2)$ are obtained from the asymptotic behavior Eqs. (67), (68), and (71). Similarly, we have

$$\frac{\partial}{\partial y}\left(\frac{I}{y}\right)_{x\to 0} \simeq x^{-1} f_0(\zeta^2) + O(1),$$

where $f_0(\zeta^2)$ is a well-defined function. Note that the singularity vanishes already after the first differentiation with respect to γ.

V. CALCULATION OF THE OBSERVABLES

In addition to the population of the various bound states calculated in the previous section, we show here how to calculate the energy spectrum of the ejected electron. We first note that, by contrast to the pure Coulomb potential, our separable potential has a short range. This means that we can use the Lippmann-Schwinger equation to build the continuum state $|\varphi_k^{\pm}\rangle$ of wave vector $\vec{k}$. The normalization which is adopted here is such that the scalar product of two plane waves writes as follows:

$$\langle\vec{p}'|\vec{p}\rangle = (2\pi)^3\delta(\vec{p}' - \vec{p}). \quad (73)$$

Upon this condition, the wave function in momentum space of the continuum state $|\varphi_k^{\pm}\rangle$ writes

$$\langle\vec{p}|\varphi_k^{\pm}\rangle = \varphi_k^{\pm}(\vec{p}) = (2\pi)^3\delta(\vec{p} - \vec{k}) + \chi_k^{\pm}(\vec{p}), \quad (74)$$

where

$$\chi_k^{\pm}(\vec{p}) = \frac{2}{(k \pm i\epsilon)^2 - p^2}\int \frac{d\vec{p}'}{(2\pi)^3} V(\vec{p},\vec{p}')\varphi_k^{\pm}(\vec{p}'). \quad (75)$$

$V(\vec{p},\vec{p}')$ is given by Eq. (5). The upper scripts + and − refer to an outgoing and an ingoing wave behavior, respectively. The ionization amplitude writes

$$C(\vec{k},t) = \langle\varphi_k^-|\Phi(t)\rangle. \quad (76)$$

The differential probability for an electron having the energy E is determined in terms of the spectral density $D(E,t)$:

$$dP = D(E,t)\,dE, \quad (77)$$

where

$$D(E,t) = \frac{\sqrt{2E}}{(2\pi)^3}\int |C(\vec{k},t)|^2 d\Omega_k, \quad (78)$$

with Ω_k denoting the solid angle under which the electron is emitted. Obviously, the total ionization yield is equal to

$$P(t) = \int_0^\infty D(E,t)\,dE = 1 - |C_{1s}(t)|^2 - |C_{2s}(t)|^2 - \sum_{m=-1}^{1} |C_{2p,m}(t)|^2. \quad (79)$$

VI. NUMERICAL IMPLEMENTATION

In this section, we briefly describe the technique implemented to solve numerically the linear Volterra integral equation:

$$f(t) = g(t) + \int_0^t dy K(t,y) f(y), \quad 0 \leqslant t \leqslant T. \quad (80)$$

This method which combines a block-by-block integration technique and the Simpson interpolation formula, was developed several years ago by Linz [23]. However, its implementation in the present case, requires one to rewrite the kernel $K(t,y)$ as follows:

$$K(t,y) = C_K + \sqrt{t-y}K^{(c)}(t,y), \quad (81)$$

where $K^{(c)}(t,y)$ is a smooth and continuous function and C_K a constant. As a result, Eq. (80) becomes

$$f(t) = g(t) + C_K\int_0^t dy f(y) + \int_0^t dy\sqrt{t-y}K^{(c)}(t,y)f(y). \quad (82)$$

In order to implement the Linz method, we proceed as follows. We first subdivide the time interval $[0,t]$ into equal subintervals $[t_j,t_{j+2}]$ of length $2h$ with $j = 0,\ldots,N-2$, N being an even number. Each subinterval $[t_j,t_{j+2}]$ is further subdivided into equal subintervals $[t_{j0},t_{j2}]$ with $t_{jl} = t_j + lh$, $l = 0,1,2$. In each subinterval $[t_j,t_{j+2}]$, we use a three-point (t_{j0},t_{j1} and t_{j2}) Lagrange interpolation to approximate the well-behaved part of the integrand, namely $K^{(c)}(t,y)f(y)$. We then perform the change of variable $y = t_j + uh$ and integrate analytically over u in each subinterval $[t_j,t_{j+2}]$. After some manipulations, we obtain

$$\int_0^{t_i} dy\sqrt{t_i - y}K^{(c)}(t_i,y)f(y) \approx h^{3/2}\sum_{j=0}^{i-2}[\alpha(t_i - t_j)K^{(c)}(t_i,t_j)f(t_j) + \beta(t_i - t_j)K^{(c)}(t_i,t_{j+1})f(t_{j+1}) + \gamma(t_i - t_j)K^{(c)}(t_i,t_{j+2})f(t_{j+2})], \quad (83)$$

where the functions α, β, and γ take the following form:

$$\alpha(k) = \frac{1}{2}\int_0^2 (1-u)(2-u)\sqrt{k-u}\ du, \tag{84}$$

$$\beta(k) = \int_0^2 u(2-u)\sqrt{k-u}\ du, \tag{85}$$

$$\gamma(k) = \frac{1}{2}\int_0^2 u(u-1)\sqrt{k-u}\ du. \tag{86}$$

The remaining integral in Eq. (82) can be calculated by means of the well-known Simpson's rule. In order to simplify the notations, we write $g_i \equiv g(t_i)$, $F_i \equiv f(t_i)$, and $K^{(c)}(t_i,t_j) \equiv K^{(c)}_{i,j}$. After some manipulations, we obtain the following system of equations to solve for the unknowns F_{2m+1} and F_{2m+2}:

$$\begin{aligned} F_{2m+1} &= g_{2m+1} + hC_K \sum_{i=0}^{2m} \varpi_i F_i \\ &+ \frac{1}{6}hC_K[F_{2m} + 4F_{2m+1/2} + F_{2m+1}] \\ &+ h^{3/2}\sum_{l=0}^{m-1}\big[\alpha(2m+1-2l)K^{(c)}_{2m+1,2l}F_{2l} \\ &+ \beta(2m+1-2l)K^{(c)}_{2m+1,2l+1}F_{2l+1} \\ &+ \gamma(2m+1-2l)K^{(c)}_{2m+1,2l+2}F_{2l+2}\big] \\ &+ \left(\frac{1}{2}h\right)^{3/2}\big[\alpha(2)K^{(c)}_{2m+1,2m}F_{2m} + \beta(2)K^{(c)}_{2m+1,2m+1/2} \\ &\times F_{2m+1/2} + \gamma(2)K^{(c)}_{2m+1,2m+1}F_{2m+1}\big], \end{aligned} \tag{87}$$

$$\begin{aligned} F_{2m+2} &= g_{2m+2} + hC_K \sum_{i=0}^{2m} \varpi_i F_i \\ &+ \frac{1}{3}hC_K[F_{2m} + 4F_{2m+1} + F_{2m+2}] \\ &+ h^{3/2}\sum_{l=0}^{m-1}\big[\alpha(2m+2-2l)K^{(c)}_{2m+2,2l}F_{2l} \\ &+ \beta(2m+2-2l)K^{(c)}_{2m+2,2l+1}F_{2l+1} \\ &+ \gamma(2m+2-2l)K^{(c)}_{2m+2,2l+2}F_{2l+2}\big] \\ &+ h^{3/2}\big[\alpha(2)K^{(c)}_{2m+2,2m}F_{2m} + \beta(2)K^{(c)}_{2m+2,2m+1}F_{2m+1} \\ &+ \gamma(2)K^{(c)}_{2m+2,2m+2}F_{2m+2}\big], \end{aligned} \tag{88}$$

where $\varpi_i = \frac{1}{3}\{1,4,2,\ldots,2,4,1\}$ and $t_{2m+1/2} = t_{2m} + \frac{1}{2}h$. To deal with the unknown value $F_{2m+1/2}$ we approximate it by quadratic interpolation, using values $F_{2m}, F_{2m+1}, F_{2m+2}$, that is, we write

$$F_{2m+1/2} \simeq \tfrac{3}{8}F_{2m} + \tfrac{3}{4}F_{2m+1} - \tfrac{1}{8}F_{2m+2}.$$

Starting with $F_0 = g_0$, we solve Eqs. (87) and (88) successively for blocks of values $(F_1,F_2),(F_3,F_4),\ldots$, using standard BLAS and LAPACK library programs.

VII. VALIDATION OF THE MODEL

In order to validate our model and check the pertinence of the present choice of the separable potentials, we consider in this section several physical situations where the electron dynamics in strong oscillating fields are well known. In all our calculations, we take into account the three bound states $1s$, $2s$, and $2p$ and assume that the model atom is initially in its ground state. We first calculate by means of Eq. (79), the probability of ionization of our model atom as a function of the peak field intensity. We consider the case of an eight-optical-cycle pulse of 0.6 a.u. photon energy. The results are presented in Fig. 1. At low peak field intensity, only one photon is necessary to ionize the atom. According to the lowest order of the perturbation theory, the ionization probability should be proportional to the peak intensity giving a straight line on a *log-log* plot. At low peak intensity, our results for the probability of ionization coincides with the straight dashed line of slope exactly one. For higher peak intensities, above 3×10^{14} W/cm^2, multiphoton transitions occur before reaching an intensity regime where saturation takes place and nonperturbative effects are important. As a matter of fact, nonperturbative effects become important when the ponderomotive potential U_p exceeds the photon energy ω. In Fig. 1, the green vertical dashed line indicates the value of the peak intensity, namely 3×10^{16}W/cm^2 that corresponds to $U_p = \omega$. In Fig. 2, we show the spectrum resulting from the interaction of our model atom with an eight-optical-cycle pulse of 10^{15}W/cm^2 for the peak intensity and 1 a.u. for the photon energy. The spectrum exhibits several ATI peaks separated by the photon energy as expected. Among the ATI peaks, the first one is by far the dominant one. It is due to the absorption of

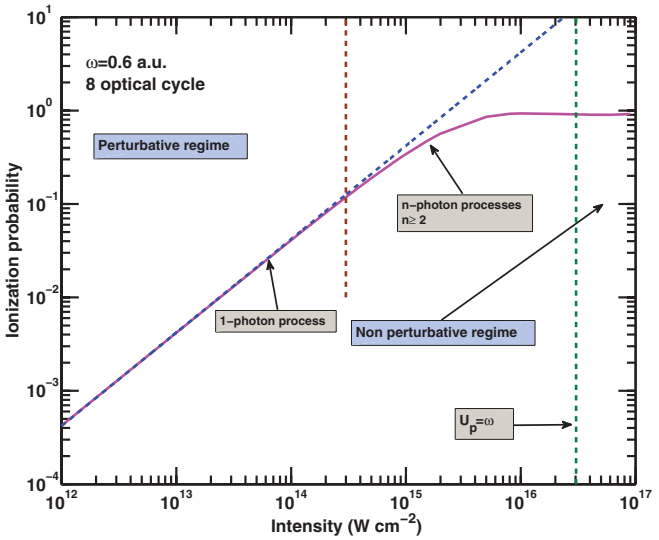

FIG. 1. (Color online) Probability of ionization of our model atom initially in the $1s$ state, as a function of the peak field intensity (solid line). The total duration of the pulse is eight-optical cycle and the photon energy is 0.6 a.u. The blue dashed straight line has a slope exactly equal to 1. The vertical brown dashed line delimits the intensity region where one-photon processes dominate. The vertical green dashed line corresponds to an intensity of 3×10^{16}W/cm^2 for which $U_p = \omega$ in a.u. For larger peak intensities, the interaction of the atom with the field is predominantly nonperturbative.

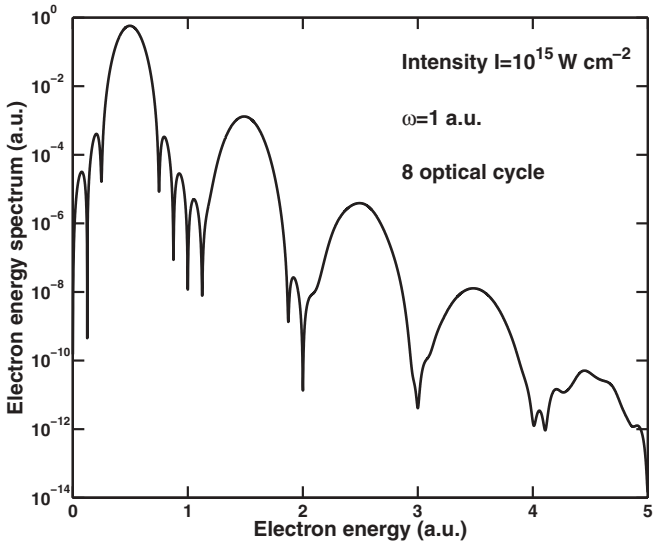

FIG. 2. Electron energy spectrum resulting from the interaction of our model atom, initially in the $1s$ state, with an eight-optical cycle sine square pulse. The peak intensity is equal to $10^{15}\mathrm{W/cm^2}$ and the photon energy, to 1 a.u.

a single photon. The satellite peaks on both sides of the first ATI peak result from the fact that the density of probability is proportional to the square of the Fourier transform of the sine square pulse [see Eq. (3)].

The third situation we are dealing with is the interaction of our model atom with a long and intense pulse of 0.375 a.u. photon energy. Since this photon energy corresponds to the $1s$-$2p$ transition frequency, the coupling of the external field to the atom is resonant. Rabi oscillations and the Autler-Townes effect are expected to manifest in the time evolution of the atomic state populations and in the ATI spectrum, respectively.

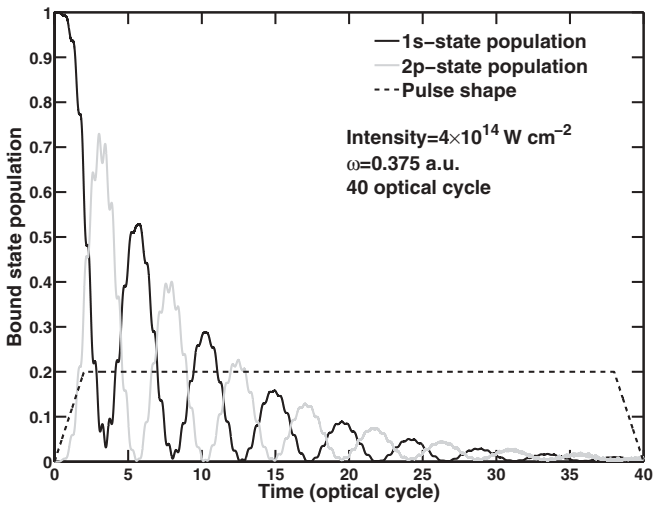

FIG. 3. Rabi oscillations of the $1s$ (black line) and $2p$ (gray line) state populations as a function of time. Our model atom which is assumed initially in the $1s$ state, interacts with a laser pulse whose frequency is equal to the $1s$-$2p$ transition frequency. The pulse is turned on and off linearly over two optical cycles and has a flat top of 36 optical cycles. The pulse shape (dashed line) is shown in arbitrary units. The peak intensity is equal to $4 \times 10^{14}\mathrm{W/cm^2}$.

In this case where only two states play a significant role, it makes sense to compare the results of our model, both qualitatively and quantitatively to those obtained by solving the TDSE with no approximation on the Coulomb potential. In the following, we assume that the laser pulse is turned on and off linearly over two optical cycles and has a flat top of 36 optical cycles. The peak intensity is equal to $4 \times 10^{14}\mathrm{W/cm^2}$. In Fig. 3, we show the time evolution of the population of the "bare" atomic states $1s$ and $2p$. As expected, these populations exhibit Rabi oscillations. Since these oscillations occur during the time the field intensity is constant and equal to the peak intensity, we can estimate the corresponding Rabi frequency. We obtain $\Omega_{\mathrm{Rabi}} = 0.08$ a.u. Exactly at resonance, the expression of the Rabi frequency is given by

$$\Omega_{\mathrm{Rabi}} = \mathcal{E}\langle 1s|z|2p\rangle, \tag{89}$$

where $\mathcal{E}$ is the field amplitude. In the present case, we find $\Omega_{\mathrm{Rabi}} = 0.0795$ a.u. in very good agreement with the estimated value. The Rabi oscillations shown in Fig. 3 are damped. This is due to the coupling of both the $2s$ and the $2p$ state to the continuum which is fully taken into account in our model. This coupling to the continuum leads to the well-known Autler-Townes effect in the electron energy spectrum [24–26]. This effect is shown in Fig. 4 for the same laser parameters. We clearly observe a splitting of each ATI peak. We have checked that the energy separation between the subpeaks of each Autler-Townes doublet is exactly equal to the Rabi frequency. Let us now analyze the behavior of each Autler-Townes doublet in more detail for increasing peak intensities. In Fig. 5, we show the first ATI peaks for the same laser parameters as before but for various peak field intensities. As the peak intensity increases, the subpeaks of the Autler-Townes doublets move apart. This of course is

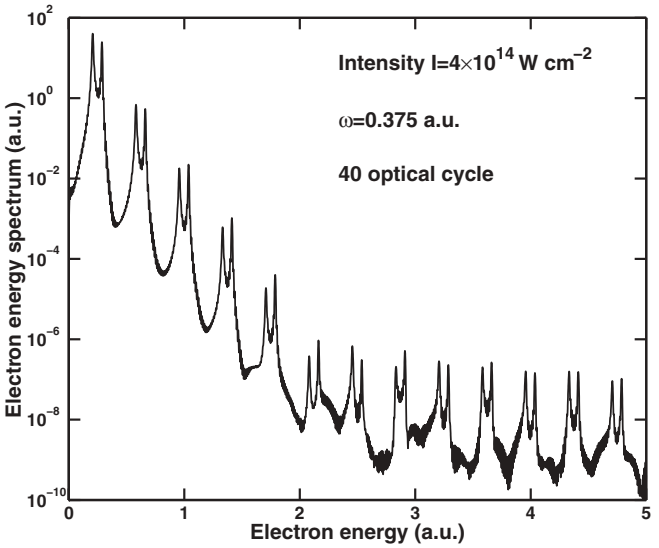

FIG. 4. Electron energy spectrum resulting from the interaction of our model atom, initially in the $1s$ state, with a pulse whose peak electric field is equal to $\mathcal{E}_0 = 0.107$ a.u. and the frequency equal to $\omega = 0.375$ a.u. The pulse has a trapezoidal shape with a two-optical cycle linear turn on and off and a 36-optical cycle flat top.

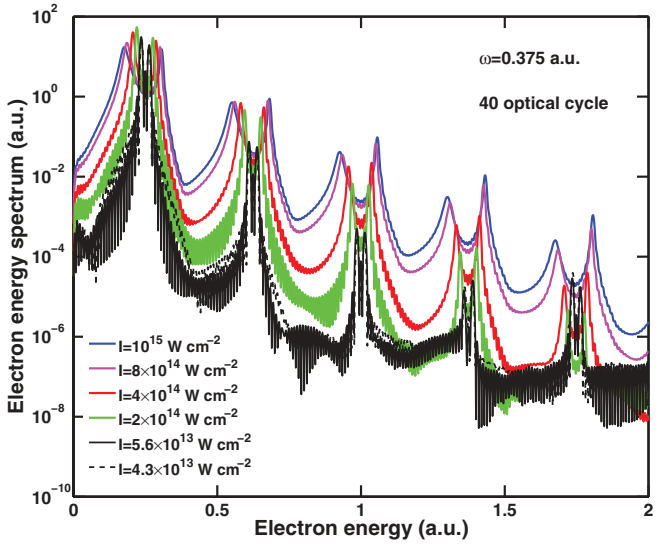

FIG. 5. (Color online) Electron energy spectra resulting from the interaction of our model atom, initially in the 1s state, with laser pulses of 0.375 a.u. photon energy. All pulses have the same trapezoidal shape as in Fig. 3 but various peak field intensities (given in the lower left part of the graph) are considered.

expected since the Rabi frequency increases with the peak intensity. Another interesting feature that we observe in the energy spectra is the fact that while the intensity is increasing, the left subpeak of each Autler-Townes doublet gets broader in contrast to the right subpeak whose width hardly changes. This effect of power broadening is clearly shown in Fig. 6 where the first Autler-Townes doublet is presented on a linear scale for two different peak intensities.

Within a quantized field picture in which we assume for the time being that the atom-field interaction is switched off, the dressed state energy spectrum is made of a ladder of pairs

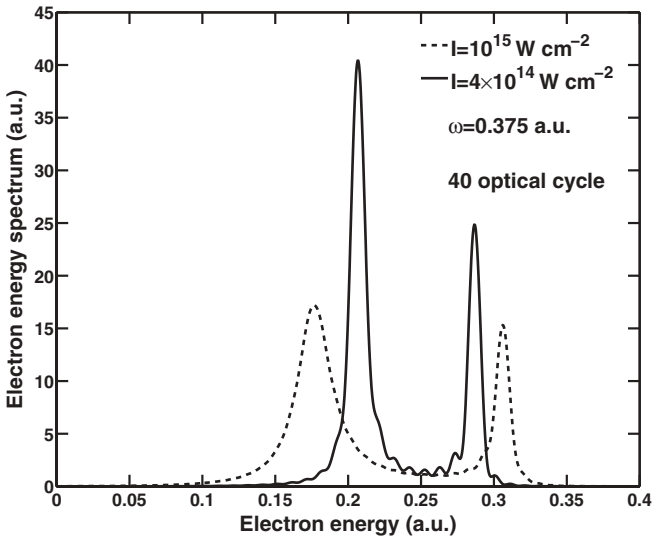

FIG. 6. Electron energy spectrum resulting from the interaction of our model atom, initially in the 1s state with the same laser pulse as in Fig. 5, for two peak intensities: 10^{15} W/cm^2 (dashed line) and 4×10^{15} W/cm^2 (solid line). The figure shows the first ATI peak of the electron energy spectrum on a linear scale.

of states $|1s,(n+1)\omega\rangle$ and $|2p,n\omega\rangle$ of the atom-field system. n gives the number of photons involved at each step of the ladder. If the field frequency is exactly on resonance with the atomic transition frequency, these unperturbed dressed states are degenerate in energy. If we now switch on the atom-field interaction, the degeneracy is lifted up leading to pairs of dressed states separated in energy by the Rabi frequency. These dressed states are in fact linear superpositions of the unperturbed $|1s,(n+1)\omega\rangle$ and $|2p,n\omega\rangle$ states. It is the coupling of these dressed states to the atomic continuum that leads to the Autler-Townes effect (i.e., to the splitting of each ATI peak into a doublet). The width of the subpeaks of each doublet depends on the coupling strength of the dressed states to the continuum or in other words, on the ionization rate of each of the dressed states. The results presented in Figs. 5 and 6 suggest that for each pair of dressed state energy levels, the rate of ionization of the lower state is higher than the one of the upper state.

In order to check that this result is not an artefact of the present model, we have performed Floquet calculations in the case of atomic hydrogen. These calculations have been obtained by means of a representation in a basis of Sturmian functions of the Floquet operator associated with the Hamiltonian of atomic hydrogen interacting with a periodic field of fixed frequency ω and intensity I in the velocity gauge [27,28]. By complex rotating the Hamiltonian, it is possible to identify the resonances of the system with the complex eigenvalues E of the rotated Floquet operator: the energy is given by Re(E) while the decay rate is -2Im(E) [27–29]. The results are presented in Fig. 7 for the same intensity as before, namely 4×10^{14} W/cm^2. This figure is made of three panels. In the top panel, we show the energy of the relevant Floquet

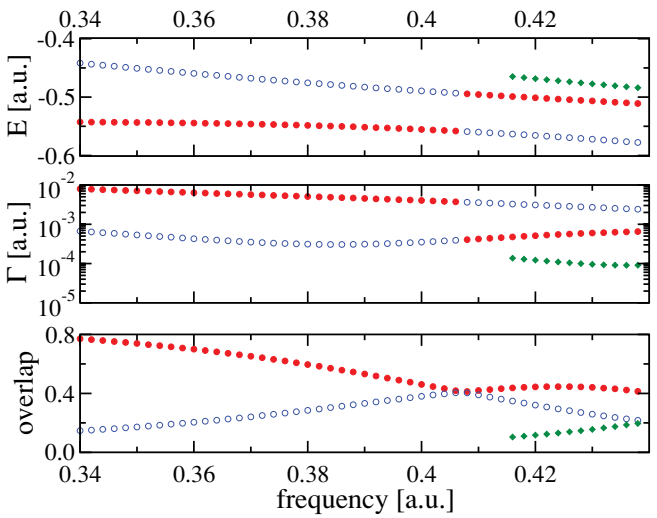

FIG. 7. (Color online) Real parts of the complex Floquet energies as a function of the frequency ω for a laser peak intensity of 4×10^{14}W/cm^2 (top panel), the corresponding ionization rates (middle panel), and the overlaps between these Floquet states and the "bare" atomic states $|1s\rangle$ and $|2p\rangle$ (bottom panel). The red solid circles correspond to a Floquet state that has the largest overlap with the $|1s\rangle$ state while the blue open circles correspond to the second largest overlap with the $|1s\rangle$ state and the first largest overlap with the $|2p\rangle$ state.

states. The middle panel shows the corresponding decay rates and the bottom panel shows the overlaps of these Floquet states with the bare atomic states. In the three panels, the Floquet states associated with the red solid circles exhibit the largest overlap and can be identified with the $|1s\rangle$ state. The blue open circles correspond to the second largest overlap with the $|1s\rangle$ state and to the first largest overlap with the $|2p\rangle$ state. Note that above $\omega = 0.415$ a.u., there is a third state whose overlap with the $|1s\rangle$ state becomes relevant (larger than 0.1). This Floquet state indicates that in the pure Coulomb states, the influence of atomic states that are not resonantly coupled to the ground state becomes important. In the top panel of Fig. 7, we observe an avoided crossing of the Floquet energies at a frequency slightly higher than the transition frequency at 0.375 a.u. This explains why for $\omega = 0.375$ a.u., the contribution of the bare $|1s\rangle$ and $|2p\rangle$ atomic states to the dressed or Floquet states is not symmetric (see the bottom panel of Fig. 7) as it should be exactly at resonance. The energies of the dressed states with larger overlap with the $|1s\rangle$ and $|2p\rangle$ states at $\omega = 0.375$ a.u. are $E_{1s} = -0.5472$ a.u. and $E_{2p} = -0.4716$ a.u. Due to the periodicity of the Floquet spectrum the Floquet states associated with the energies E and $E + k\omega$, k some integer number, correspond to the same physical state. The positions of the left and right subpeaks in Fig. 6 are quite close to $E_{1s} + 2\omega = 0.2028$ and $E_{2p} + 2\omega = 0.2784$, respectively. This indicates that the $|1s\rangle$ ($|2p\rangle$) state is more dominant in the left (right) subpeak. Finally, at $\omega = 0.375$ a.u., we see in the middle panel that the ionization rates of both Floquet states differ by one order of magnitude. Consequently, it is expected that the left subpeak of the Autler-Townes doublet is broader than the right one. These results confirm those of Girju *et al.* [26] and show that in the present physical situation, the predictions of our model are qualitatively correct. In Fig. 8, we compare the first ATI peaks obtained with our model, to those calculated by solving numerically the TDSE for atomic hydrogen [30]. The agreement is quantitatively relatively good as expected since mainly two states, $|1s\rangle$ and $|2p\rangle$, are dominating the dynamics.

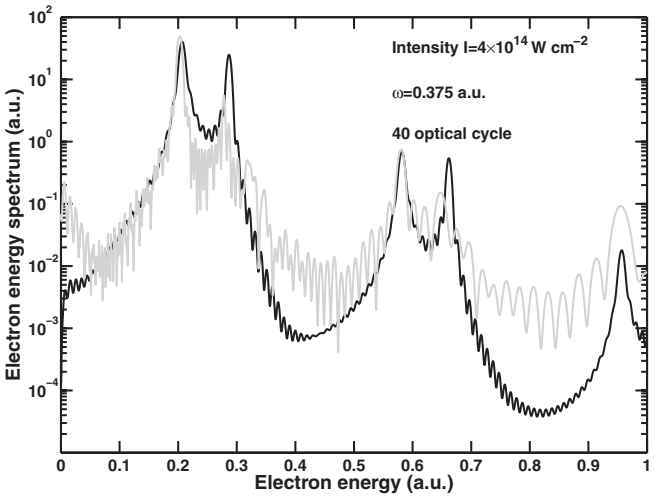

FIG. 8. Electron energy spectrum resulting from the interaction of our model atom initially in the $|1s\rangle$ with a laser pulse of 0.375 a.u. photon frequency and of 4×10^{14}W/cm^2 peak intensity. The laser pulse shape is trapezoidal with a two-cycle linear turn on and off and with a flat top of 36 optical cycles. The gray line is the result obtained by solving numerically the time-dependent Schrödinger equation while the black line is the result obtained with our model.

VIII. CONCLUSIONS

In this contribution, we considered the ionization of atomic hydrogen by an intense infrared pulse. We solved the corresponding TDSE in momentum space when the kernel of the nonlocal Coulomb potential is replaced by a finite sum of separable potentials, each of them supporting one bound state of atomic hydrogen. Such an approach bears some resemblance to a spectral method. However, instead of the usual expansion of the solution of the TDSE in terms of a finite set of L^2-integrable functions, it is the potential kernel which is now expanded in terms of separable potentials. The choice of these separable potentials, however, is not unique and requires attention to avoid any unphysical effects. This approach has significant advantages when it is compared to the well-established SFA. By contrast to the SFA, it provides a rigorous solution for the electron wave packet, it includes more than one bound states, it takes fully into account the continuum-continuum transitions, and, more important, it is fully gauge invariant. In addition, we have shown that this model allows one to reduce the three-dimensional Schrödinger equation to a small system of coupled one-dimensional linear Volterra integral equations, the numerical solution of which is relatively easy to obtain. In order to validate the model, we have checked that in the perturbative regime, when the ponderomotive potential is smaller than the laser frequency, the corresponding behaviors of the ionization yield and the ATI spectrum are well reproduced. Furthermore, we have shown that the resonant coupling of the $1s$ to the $2p$ states leads to Rabi oscillations of the corresponding populations at the correct frequency as well as to a Rabi splitting of the ATI peaks.

The main objective of the present contribution is to provide a theoretical tool to understand the actual role of the atomic potential in the intensity regime where tunnel ionization is supposed to take place and where the experimental data for the first ATI peaks are in contradiction with the theoretical predictions based on the SFA model. This problem will be the subject of a forthcoming publication.

ACKNOWLEDGMENTS

One of the authors (H.M.T.N.) gratefully acknowledges the financial support of the International Atomic Energy Agency (IAEA) through the Abdus Salam ICTP (International Centre for Theoretical Physics)-IAEA Sandwich Training Educational Programme (STEP). M.G.K.N. is grateful to the Abdus Salam ICTP for its support through the OEA-AC-71 project. M.G.K.N. and Yu.V.P. thank the Université Catholique de Louvain for hospitality and financial support. The authors thank the Université Catholique de Louvain for providing them with access to the supercomputer of the Calcul Intensif et Stockage de Masse (CISM) which is supported by the Fonds

National de la Recherche Scientifique (FNRS) through the Fonds de la Recherche Fondamentale et Collective (FRFC) Project No 2.4556.99, "Simulations Numériques et traitement des données."

APPENDIX

All basic functions $J_{\mu\nu}$ defined in (25) and (40) can be expressed by means of the function $I(x,y;\gamma)$ and its derivatives. We have

$$J_{11}(x,y) = -\frac{16}{\pi i y}\left[\frac{1}{3!}\frac{\partial^3}{\partial\gamma^3} I(x,y;\gamma)\right]_{\gamma=1}, \tag{A1}$$

$$J_{12}(x,y) = \frac{4\sqrt{2}}{\pi i y}\left[\left(\frac{\partial^2}{\partial\beta\partial\gamma} + \frac{1}{2\times 2!}\frac{\partial^3}{\partial\beta^2\partial\gamma}\right)\frac{1}{(\beta-\gamma)} \times [I(x,y;\gamma) - I(x,y;\beta)]\right]_{\gamma=1,\,\beta=1/4}, \tag{A2}$$

$$J_{22}(x,y) = -\frac{2}{\pi i y}\left[\left(\frac{1}{3!}\frac{\partial^3}{\partial\beta^3} + \frac{1}{4!}\frac{\partial^4}{\partial\beta^4} + \frac{1}{4\times 5!}\frac{\partial^5}{\partial\beta^5}\right) \times I(x,y;\beta)\right]_{\beta=1/4}, \tag{A3}$$

$$J_{13}(x,y) = -\frac{8}{\sqrt{2}\pi\ i y}\frac{\partial^3}{\partial\beta^2\partial\gamma}\left[\frac{1}{(\beta-\gamma)}[I(x,y;\gamma) - I(x,y;\beta)]\right]_{\gamma=1,\,\beta=1/4}, \tag{A4}$$

$$J_{23}(x,y) = \frac{4}{\pi i y}\left[\left(\frac{1}{4!}\frac{\partial^4}{\partial\beta^4} + \frac{1}{2\times 5!}\frac{\partial^5}{\partial\beta^5}\right) I(x,y;\beta)\right]_{\beta=1/4}, \tag{A5}$$

$$J_{33}(x,y) = -\frac{48}{\pi\ i y}\left[\frac{1}{6!}\frac{\partial^5}{\partial\beta^5} I(x,y;\beta)\right]_{\beta=1/4}. \tag{A6}$$

[1] E. Huens, B. Piraux, A. Bugacov, and M. Gajda, Phys. Rev. A **55**, 2132 (1997).
[2] L. A. Collins and A. L. Merts, Phys. Rev. A **40**, 4127 (1989).
[3] X. Tang, H. Rudolph, and P. Lambropoulos, Phys. Rev. Lett. **65**, 3269 (1990).
[4] M. Pont, D. Proulx, and R. Shakeshaft, Phys. Rev. A **44**, 4486 (1991).
[5] C. Cerjan and K. Kulander, Comput. Phys. Commun. **63**, 529 (1991).
[6] E. Cormier, H. Bachau, and J. Zhang, J. Phys. B **26**, 4449 (1993).
[7] K. C. Kulander, Phys. Rev. A **35**, 445 (1987).
[8] K. C. Kulander and B. W. Shore, J. Opt. Soc. Am. B **7**, 502 (1990).
[9] A. de Bohan, B. Piraux, L. Ponce, R. Taïeb, V. Véniard, and A. Maquet, Phys. Rev. Lett. **89**, 113002 (2002).
[10] L. V. Keldysh, Zh. Eksp. Teor. Fiz. **47**, 1945 (1964) [Sov. Phys. JETP **20**, 1307 (1965)].
[11] P. B. Corkum, Phys. Rev. Lett. **71**, 1994 (1993).
[12] M. Lewenstein, Ph. Balcou, M. Yu. Ivanov, A. L'Huillier, and P. B. Corkum, Phys. Rev. A **49**, 2117 (1994).
[13] M. Lewenstein, K. C. Kulander, K. J. Schafer, and P. H. Bucksbaum, Phys. Rev. A **51**, 1495 (1995).
[14] A. Rudenko, K. Zrost, C. D. Schröter, V. L. B. de Jesus, B. Feuerstein, R. Moshammer, and J. Ullrich, J. Phys. B **37**, L407 (2004).
[15] A. de Bohan, Ph.D. thesis, Université Catholique de Louvain, Belgium, 2001.
[16] L. B. Madsen, Phys. Rev. A **65**, 053417 (2002).
[17] H. M. Tetchou Nganso, S. Giraud, B. Piraux, Yu. V. Popov, and M. G. Kwato Njock, J. Elect. Spect. Rel. Phen. **161**, 178 (2007).
[18] V. Bargmann, Rev. Mod. Phys. **21**, 488 (1949).
[19] S. Weinberg, Phys. Rev. **131**, 440 (1963).
[20] S. Giraud, B. Piraux, Yu. V. Popov, and H. M. Tetchou Nganso, in *Proceedings of SPIE "Saratov Fall Meeting–SFM'05: Laser Physics and Photonics, Spectroscopy and Molecular Modelling VI,"* edited by V. L. Derbov, L. A. Melnikov, and L. M. Babkov, Vol. 6165, 61650D-1 (2006).
[21] *Handbook of Mathematical Functions, NBS Applied Mathematical Series*, edited by M. Abramowitz and I. A. Stegun (National Bureau of Standards, Washington DC, 1966).
[22] I. S. Gradshteyn and I. M. Ryzhik, *Table of Integrals, Series, and Products*, 7th ed, edited by Alan Jeffrey and Daniel Zwillinger (Elsevier Academic Press, Boston, 2007).
[23] P. Linz, *Analytical and Numerical Methods for Volterra Equations* (SIAM, Philadelphia, 1985).
[24] S. H. Autler and C. H. Townes, Phys. Rev. **100**, 703 (1955).
[25] P. L. Knight, J. Phys. B **12**, 3297 (1979).
[26] M. G. Girgu, K. Hristov, O. Kidun, and D. Bauer, J. Phys. B **40**, 4165 (2007).
[27] R. M. Potvliege and R. Shakeshaft, Phys. Rev. A **38**, 1098 (1988).
[28] A. Buchleitner, D. Delande, and J. C. Gay, J. Opt. Soc. Am. B **12**, 505 (1994).
[29] J. Madroñero and A. Buchleitner, Phys. Rev. A **77**, 053402 (2008).
[30] J. Madroñero and B. Piraux, Phys. Rev. A **80**, 033409 (2009).